Electrical Power and Energy Systems 156 (2024) 109726

Contents lists available at ScienceDirect

International Journal of Electrical Power and Energy Systems

journal homepage: www.elsevier.com/locate/ijepes

Hybrid state-estimation in combined heat and electric network using SCADA and AMI measurements

Vedantham Lakshmi Srinivas [a], Jianzhong Wu [b,*], Bhim Singh [c], Sukumar Mishra [c]

[a] Department of Electrical Engineering, Indian Institute of Technology (Indian School of Mines) Dhanbad, 826004, India
[b] Head of School Office, School of Engineering, Cardiff University, Cardiff, CF24 3AA, United Kingdom
[c] Department of Electrical Engineering, Indian Institute of Technology Delhi, New Delhi 110016, India

ARTICLE INFO

Keywords:
Integrated energy system
Kalman filter
Neural network
Smart local energy systems and state estimation

ABSTRACT

State-estimation plays a vital role to monitor, observe and understand the combined heat and electric network. In this paper, a hybrid framework is presented to accurately estimate the system states of electric distribution network and heat network, using the limited non-redundant measurements obtained from supervisory control and data acquisition and advanced metering infrastructure systems. The presented hybrid framework involves two steps, namely, the state-forecasting and the state-estimation. The state-forecasting uses a deep neural network to forecast the system states at every fifteen minutes interval, while these forecasted states are further used by the hybrid estimator, which uses a robust extended Kalman filter to estimate the system states with help of both datasets corresponding to supervisory control and data acquisition and advanced metering infrastructure systems, at hourly interval. The proposed framework does not completely rely on the system model at different instants. The effectiveness of the method is validated through thorough comparisons with simulation studies carried out using the Barry Island test system, United Kingdom. Satisfactory performance is observed even with the presence of bad data in the measurements.

1. Introduction

Nowadays, the integration of the heat and electrical energy networks is booming in order to deliver reliable and cost-effective energy services with reduced impact on the environment [1]. The integrated energy networks are very flexible to improve the system performance through implementation of energy hubs, where multiple energy carriers at the ports are transformed to provide certain required energy services in a coordinated manner [2,3]. Thus integrated energy networks are emerging as a promising solution to obtain optimal dispatch of multi-carrier energy systems to effectively reduce the energy consumption [4,5]. The current status of heat pumps, related energy policies, and future challenges of having coordinated heat and electrical energy systems are summarized in [6], wherein the comprehensive analysis on ancillary services of integrated heat and electrical energy systems is also discussed to maintain reliability and flexibility in the system operation.

The electric network and district heat network can communicate with one another when additional coupling elements such as CHPs are connected, which collectively form CHEN [7,8]. Research has been performed on accomplishing various essential objectives through integrated electric and heat network analysis, such as improving demand side management, operator cost minimization, optimal scheduling, etc. [9,10]. This requires the network control scheme to have real-time knowledge about the topology and the states of the CHEN [11]. State estimation in CHEN therefore, plays pivot role for the network operator in monitoring the system and taking appropriate control decisions [12].

Traditionally, the state estimation task is usually accomplished through model-based approaches using WLS estimation in power systems [13,14]. This approach has been replicated in the CHEN systems. For instance Sun et al. [15] have performed the state-estimation in CHEN using the measurements acquired from the SCADA system, however, the comprehensive measurement data is considered, usually not available in practical networks. The redundancy in the network measurements is desirable for precise state-estimation and the coupling components such as CHPs contribute to increasing system redundancy as they provide linkages between the electric and heat networks. Li et al. [16] have analyzed the impact of installation locations of coupling components in the CHEN energy flow calculation. Nevertheless, the measurements redundancy in CHEN is still low and consequently it becomes difficult for the traditional model based approach to accurately estimate the network states [17]. To address this redundancy

* Corresponding author.
E-mail addresses: vlsrinivas@iitism.ac.in (V.L. Srinivas), wuj5@cardiff.ac.uk (J. Wu), bsingh@ee.iitd.ac.in (B. Singh), sukumar@ee.iitd.ac.in (S. Mishra).

https://doi.org/10.1016/j.ijepes.2023.109726
Received 19 June 2023; Received in revised form 5 October 2023; Accepted 12 December 2023
Available online 21 December 2023

List of Abbreviations and Acronyms

AMEE	Absolute mean estimated errors
AMFE	Absolute mean forecasted error
AMI	Advanced metering infrastructure
ANN	Artificial neural network
CHEN	Combined heat and electric network
CHP	Combined heat and powerplant
DNN	Deep neural network
EKF	Extended Kalman filter
LV	Low-voltage
MSE	Mean square error
MV	Medium-voltage
OS	Operating system
PMU	Phasor measurement unit
RAM	Random access memory
SCADA	Supervisory control and data acquisition
WLS	Weighted least squares
WLAV	Weighted least absolute value

issue, Zang et al. [18] have proposed a pseudo-measurement model to roughly predict the heat load data at different nodes and use those measurements for the state estimation purpose, using a model-based WLAV state estimator. Furthermore, the effect of including the AMI measurements is analyzed in [19] to enhance the observability of the CHEN, using the weighted least absolute value based framework. Observability is a necessary and sufficient requirement for the construction of full-state estimators. Here, the performance of the CHEN is hampered with the presence of the outliers as it is sensitive to the anomalies in the measurements. Likewise, the similar drawbacks are reported in [20] using the least square framework with second-order conic programming. Owing to this concern, the alternating direction method of multipliers-based bilinear measurement model is developed in [21,22] for the CHEN to acquire the system states with the coordinated coupling units, and improved computational efficiency [23]. These aforementioned model-based state estimation methods require detailed hydraulic modeling, thermal modeling, and modeling of coupling components of CHEN to build the relationship amongst mass flow rate, pressure, temperature, heat power and electric power [24], while considering the practical effect of variation in inlet temperature causing the delay in heat transfer [25]. Since the model-based estimators demand the complete modeling of the network dynamics and redundant measurements, solely model-based approaches for CHEN state-estimation cannot be completely relied on.

This paper proposes a hybrid state-estimation approach in CHEN, which involves a two-step process. The first step involves *state forecasting* through a DNN, while the second step uses an extended Kalman filter for obtaining accurate *state-estimation* in the network with limited measurements. The proposed approach is not completely dependent on the system model for state-estimation, neither does it requires the complete set of measurements. A trade-off approach is taken in the proposed method, where the measurements are split into the SCADA and AMI measurements. The measurements data in CHEN are usually obtained from the well-known SCADA systems and the AMI systems [26]. The AMI systems involve smart electric and heat meters, and the detailed insight and accuracy of these measurement devices are reported in [27]. The SCADA measurements are usually updated every 15 min and the AMI measurements are updated on hourly basis. The PMU data, if available, is considered at fifteen minute interval, clubbed with the SCADA measurements. If just SCADA measurement data is used, the interval time of which is about a few minutes, and the PMU data acquired (at time intervals of milli-seconds) during the SCADA data acquisition period do not participate in the state estimation, resulting in a waste of more accurate and higher refresh rate PMU data [28,29]. As a result, the researchers presented many options for integrating measurements with different sample periods of SCADA system and PMU data [30,31]. Using these methods, the SCADA measurements can be processed in synchronism with the PMU measurements. Further, the detailed time-scale characteristics for state-estimation in CHEN are analyzed in [32] using the holistic frameworks. Using either the SCADA or AMI measurements alone cannot be sufficient to perform the state-estimation of the integrated networks, as the acquired measurements lack in redundancy. Therefore, an application of the SCADA and AMI measurements together is contemplated in this work. AMI measurements data provides extremely abundant measurements data, and the meters are often only loosely time-synchronized with possible delays [33], thereby, the AMI measurements could be considered in the model as pseudo measurements. However, the AMI data processing methods [34,35] could be deployed aiming the measurement time-alignment, of data sets from distributed metering, relying on the voltage signal signature. As the SCADA measurements are updated every 15 min, the measurements are processed through a trained DNN to obtain the approximate state estimates, termed herein as state forecasting. However, when the operator has the collection of AMI measurements on hourly basis, the approximate states obtained using DNN are further processed using a robust EKF, to obtain very accurate system states. Therefore, the first state-forecasting step and the second state estimation step are sequentially carried-out. It is shown in the work that even if the AMI measurements are insufficient to render the measurements redundancy, consideration of pseudo measurements still fetch the state estimates after the second step in the proposed hybrid state estimator. In light of the discussion, the contributions of the work are as follows.

- A method of forecasting the CHEN states using only a *limited* SCADA data-set.
- A robust extended Kalman filter design for state estimation in CHEN using SCADA and AMI data-set containing some gross errors.
- A hybrid state estimation framework that handles the unsynchronized SCADA and AMI noisy-measurements obtained at different time frames.

Test results validate the proposed method on real-time data-sets of the Barry Island CHEN system of the United Kingdom. The presented framework provides excellent performance even with the bad data in the heat and electrical measurement data-sets. Comprehensive comparative results demonstrate the effectiveness of the estimation accuracy of the proposed hybrid estimator, over the state-of-art WLS and ANN based estimators. Additionally, the computational burden of proposed estimator is also presented.

The rest of the work is divided as follows. Section 2 describes the first (forecasting) step of the proposed hybrid state estimator, while Section 3 elaborates on the second step of the estimator involving s robust extended Kalman-filter based measurements processing. The description of the simulation test system, along with the detailed analysis of results and discussions, is reported in Section 4. Finally, Section 5 draws the conclusions from the presented work.

2. State forecasting using DNN

The framework of the proposed hybrid state estimation is explained in this section. A flowchart of the proposed hybrid state estimation for power distribution systems is shown in Fig. 1. The left-hand of the flowchart describes the 'training phase', where state models based on DNN are applied for the state forecasting. The DNN-based state forecasting method is employed at instants whenever SCADA measurements are updated. Because the amount of SCADA measurements in the CHEN are insufficient to provide system observability, standard model-based estimators such as WLS or WLAV may fail to produce appropriate

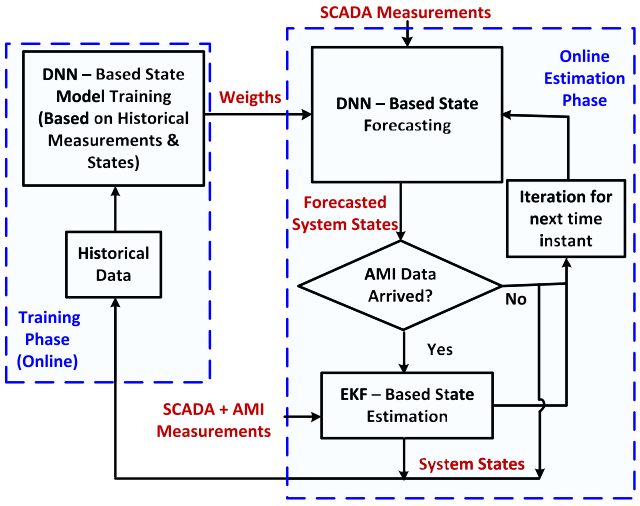

Fig. 1. Flowchart of proposed hybrid state estimator.

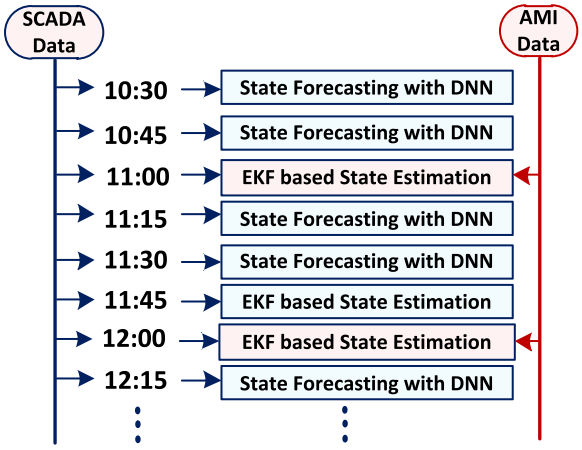

Fig. 2. Data flows and schedule of hybrid state estimation procedure.

estimation results. When both SCADA and AMI data are updated, an enhanced Kalman filter-based estimator is implemented to guarantee robust estimation results in the face of large errors. Thus, when both SCADA and AMI measurements are refreshed, EKF-based hybrid estimator is processed, to ensure robust estimation results against gross errors, as depicted in Fig. 2. SCADA measurements are assumed to be updated every fifteen minutes and the AMI data is refreshed hourly, and the methods employed at each of time instants are as shown in Fig. 2.

The DNN is adopted for the system state forecasting. Each DNN is a neural network with more than two hidden layers to imitate complex relations of distribution systems. The proposed DNN-based state model targets to update the CHEN states with a limited number of SCADA measurements. The inputs, outputs and the training of DNN are reported as follows. The input measurements constitute of,

1. Outlet temperature, T_{oi}, $i \in$ Load nodes in heat network.
2. Supply temperature, T_{si}, $i \in$ Source nodes in heat network.
3. Nodal mass flow rate, m_{qi}, $i \in$ Load nodes in heat network.
4. Active power (P_i), voltage magnitudes ($|V|_i$) and Current flows (I_{ij}); $i, j \in$ Electric network buses.

Rather than all the above-mentioned sets of measurements, *partial set of available measurements* are considered in practice due to lack of installation of sufficient metering equipment in the electric network. Using these measurements, the DNN forecasts the CHEN system states. For this purpose, a specialized DNN is used for system state forecasting with the CHEN architecture. Each DNN is a neural network with more than two hidden layers that imitates complicated distribution system relations. Unlike the conventional data-driven strategy, which uses all available measurements to reduce the computational burden of complex distribution systems [36], the proposed DNN-based state model aims to update distribution system states using just a minimal amount of SCADA observations. Because the DNN has numerous hidden layers and a high number of parameters, it may suffer from overfitting, leading in low accuracy and poor generalization performance on unanticipated data. To solve this issue, two effective strategies are used: dropout, in which units are randomly lost during the training stage, and noise, which includes injecting noise to the DNN model. Furthermore, the complicated DNN may encounter costly computational costs throughout the network training phase. The stochastic gradient descent method is used to solve this issue, as shown here.

$$Y = Y - \eta \nabla Q_i(w) \tag{1}$$

where, Y indicates the network parameters, η is the learning rate, and $\nabla Q_i(w)$ is the gradient of the subset-i. The batch size is determined by the number of samples in each subgroup. When network parameters are updated, the method uses the gradient of a subset to estimate the gradient of the whole training dataset. The DNN considered here, is a five-layer neural network with one input layer of size of measurement matrix, three hidden layers of size greater than the input layer size and one output layer of size of the state matrix of the CHEN. In addition, the dropout rate between the first and second hidden layer is considered 0.1 and dropout rate for rest hidden layers are all considered as 0.15. The noise is injected to the model through adding Gaussian distribution noise to the input data as well as the weight factors of each layer to avoid overfitting and make it as a high generalization. Fig. 3 illustrates the flow chart of the DNN-based state estimation training. The MSE [37] is used in the algorithm tabulation to estimate network losses, and 'S_n' is the number of subgroups chosen based on batch size. When all training data is processed at once, the epoch is incremented. The training of the DNN model is completed when the number of epochs surpasses the iteration threshold (it_{max}) or the MSE is less than the precision threshold (MSE_{max}).

3. Hybrid state estimation methodology

At this stage, the measurement set is composed of SCADA measurements and the available AMI data, shown as the two inputs of the 'EKF-based state estimation box in Fig. 1. The formulation of robust EKF model-based estimator that has the ability to reject erroneous measurements, is described in this section in two stages. Initial stage CHEN modeling, which is subsequently used in the second stage for problem formulation. These are explained as follows.

3.1. Modeling of CHEN

An integrated hydraulic and thermal model is used to model the district heat network. In this context, the continuity flow equation is described as [24],

$$A\dot{m} = \dot{m}_q \tag{2}$$

where A is the network incidence matrix [24] that relates the nodes to the branches; m is the vector of the mass flow (kg/s) within each pipe; m_q is the vector of the mass flow (kg/s) through each node injected from a source or discharged to a load. Thereafter, the loop pressure for entire hydraulic network is described as,

$$BKm|\dot{m}| = \sum_{i=1}^{N_{pipe}} B_{ij} k_j \dot{m}_j |\dot{m}_j| = 0 \tag{3}$$

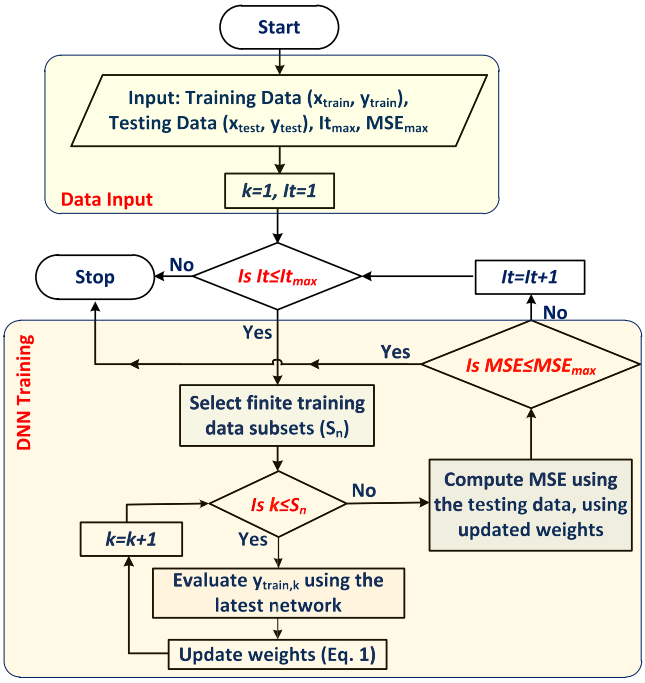

Fig. 3. DNN based state forecasting training process.

where B is the loop incidence matrix [24] that relates the loops to the branches; and where K is the vector of the resistance coefficients of each pipe. In (3), N_{pipe} is the number of pipes; 'i' is the index of loops and 'j' is the index of pipes. The three different temperatures associated with each node in the heat network include the supply temperature (T_s), the outlet temperature (T_o) and the return temperature (T_r) [38]. The heat power is described as,

$$\Phi = C_p \dot{m}_q (T_s - T_o) \tag{4}$$

where Φ is the vector of heat power consumed at each node, and C_p= 0.0042 MJ/kg/^{o}C. The temperature at the outlet of the pipe is [24],

$$T_{end} = (T_{start} - T_a) e^{-\lambda L / C_p m} + T_a \equiv T'_{end} = T'_{start} \Psi \tag{5}$$

where T_{start} and T_{end} are the temperatures at the start node and the end node of a pipe, respectively. T_a is the ambient temperature; k is the overall heat transfer coefficient of each pipe per unit length; L is the length of each pipe (m). Furthermore, $T'_{start} = T_{start} - T_a, T'_{end} = T_{end} - T_a, \Psi = e^{-\lambda L / C_p m}$. The junction/mixture temperature at a node is computed as,

$$\left(\sum \dot{m}_{out}\right) T_{out} = \left(\sum \dot{m}_{in}\right) T_{in} \tag{6}$$

where, m_{in} is the mass flow rate within a pipe coming into the node (kg/s), m_{out} is the mass flow rate within a pipe leaving the node (kg/s), T_{in} is the temperature of flow at the end of an incoming pipe and T_{out} is the mixture temperature of a node. A comparison of measurement functions with the hydraulic model equations indicates that fewer equations exist for T_s and T_r than equations for mass flow rates, and only temperature measurement equations are available for solving T_s and T_r in most instances. These factors produce many critical measurements in the heating network, where the loss of a critical measurement can result in an unobservable system, which would bear a drastic consequence of preventing the execution of the state estimator. To counter this problem, the AMI measurements are added into the state estimation model. In electric network, the active power (P_i), reactive power (Q_i) injections at bus 'i', and the current flows(I_{ij}) between two buses 'i' and 'j', for an 'n' bus electric network can be expressed as,

$$P_i = |V_i| \sum_{j=1}^{n} |V_j| (G_{ij} \cos\theta_{ij} + B_{ij} \sin\theta_{ij}) \tag{7}$$

$$Q_i = |V_i| \sum_{j=1}^{n} |V_j| (G_{ij} \sin\theta_{ij} - B_{ij} \cos\theta_{ij}) \tag{8}$$

$$I_{ij} = \sqrt{\left(G_{ij}^2 + B_{ij}^2\right)\left(|V_i|^2 + |V_j|^2 - 2|V_i||V_j| \cos\theta_{ij}\right)} \tag{9}$$

In (7) and (8), G_{ij} and B_{ij} indicate the branch conductances and susceptances in the electric network. Besides this, the coupling units considered include the CHP units, which can be modeled as follows,

$$c_{mi} = \phi_{i,source} / P_{i,CHP} \tag{10}$$

where, $\phi_{i,source}$ and $P_{i,CHP}$ are the heat and electric powers of the CHP installed at source 'i' of the network, and 'c_{mi}' is the heat-to-power ratio of the gas turbine CHP.

3.2. Problem formulation

The objective of is to precisely estimate the following network states from the SCADA and AMI measurements, obtained typically at hourly intervals. Initially, the states to be estimated, and the measurements available at this stage, are identified as follows.

- Network states to be estimated are,
  1. Mass low rates, m_{ij}, $ij \in$ All pipes in heat network.
  2. Supply temperatures, T_{si}, $i \in$ All heat load nodes.
  3. Return temperatures, T_{ri}, $i \in$ All heat load nodes.
  4. Voltage magnitudes and Voltage angles at all buses in the electric network
- Measurements data include a partial subset of,
  1. Nodal heat power consumption, Φ_i, $i \in$ Heat load nodes.
  2. Outlet temperature, T_{oi}, $i \in$ Heat load nodes.
  3. Supply temperatures, T_{si}, $i \in$ Heat source nodes.
  4. Nodal mass flow rates, m_{qi}, $i \in$ Heat load nodes.
  5. Active powers, P_i, Reactive powers, Q_i, and Voltage magnitudes ($|V|_i$), $i \in$ Electric buses.
  6. Current flows (I_{ij}) between two electric buses 'i' and 'j'

Using the modeling equations presented in the earlier subsection, the different measurements in the CHEN can be expressed in terms of the network states in the following way.

$$\boldsymbol{z_{eS}} = \boldsymbol{h_{eS}}(\boldsymbol{x_e}) + \boldsymbol{w_{eS}}; \boldsymbol{z_{hS}} = \boldsymbol{h_{hS}}(\boldsymbol{x_h}) + \boldsymbol{w_{hS}} \tag{11}$$

$$\boldsymbol{z_{eA}} = \boldsymbol{h_{eA}}(\boldsymbol{x_e}) + \boldsymbol{w_{eA}}; \boldsymbol{z_{hA}} = \boldsymbol{h_{hA}}(\boldsymbol{x_h}) + \boldsymbol{w_{hS}} \tag{12}$$

where, '$\boldsymbol{z_{eS}}$' and '$\boldsymbol{z_{eA}}$' are SCADA and AMI measurements with electrical network, while '$\boldsymbol{z_{hS}}$' and '$\boldsymbol{z_{hA}}$' are SCADA and AMI measurements with the heat network. '$\boldsymbol{x_e}$' and '$\boldsymbol{x_h}$' are state vectors with electric and heat networks respectively as follows,

$$\boldsymbol{x_e} = \begin{bmatrix} \theta_i & |V|_i \end{bmatrix} \tag{13}$$

$$\boldsymbol{x_h} = \begin{bmatrix} m_{ij} & T_{si} & T_{ri} \end{bmatrix} \tag{14}$$

In (11) and (12), $h_eS(.), h_eA(.), h_hS(.), h_hA(.)$ are the measurement vector functions as follows,

$$\boldsymbol{h_{eS}}(.) \equiv \begin{bmatrix} P_i \\ Q_i \\ I_{ij} \\ |V|_i \end{bmatrix} = \begin{bmatrix} |V_i| \sum_{j=1}^{n} |V_j| (G_{ij} \cos\theta_{ij} + B_{ij} \sin\theta_{ij}) \\ |V_i| \sum_{j=1}^{n} |V_j| (G_{ij} \sin\theta_{ij} - B_{ij} \cos\theta_{ij}) \\ \sqrt{\left(G_{ij}^2 + B_{ij}^2\right)\left(|V_i|^2 + |V_j|^2 - 2|V_i||V_j| \cos\theta_{ij}\right)} \\ |V_i|^{(k)} \end{bmatrix} \tag{15}$$

$$\boldsymbol{h_{eA}}(.) \equiv \begin{bmatrix} P_i \\ Q_i \end{bmatrix} = \begin{bmatrix} |V_i| \sum_{j=1}^{n} |V_j| (G_{ij} \cos\theta_{ij} + B_{ij} \sin\theta_{ij}) \\ |V_i| \sum_{j=1}^{n} |V_j| (G_{ij} \sin\theta_{ij} - B_{ij} \cos\theta_{ij}) \end{bmatrix} \tag{16}$$

$$\boldsymbol{h_{hS}}(.) \equiv \begin{bmatrix} \Delta p \\ T'_s \\ T'_r \end{bmatrix} = \begin{bmatrix} \sum_{i=1}^{N_{pipe}} B_{ij} k_j \dot{m}_j |\dot{m}_j| \\ C_s T'_{s,load} \\ C_r T'_{r,load} \end{bmatrix} \tag{17}$$

The vector function $\boldsymbol{h_{hA}}(.)$ is the heat power Eq. (4). Notice that the AMI measurements data in electric network is usually obtained at the LV side of secondary substations for reducing installation costs. In such case, the AMI data at the LV side is employed to derive the equivalent measurements at the MV side, along with concurrent derivation of the covariance of equivalent measurements [39]. After that, the derived measurements at the MV side are used herein. To avoid the imprecise estimation resulting due to the possible abrupt changes in the system, a robust extended Kalman filter is contemplated here. Since CHEN is a quasi-static system that changes in a slow manner, one could assume the previous estimated states would be similar to the present values and the concept of utilizing previous state values to predict the next states is plausible. A transition relationship between consecutive states could be formulated and utilized to enhance the estimation results and predict the upcoming states as well [[40]]. In grid-connected mode, any surplus or deficit in electrical power is supplied from the main grid and there is no heat generated at the electricity slack bus bar. Thus, the derivative of the heat power mismatches with respect to the electrical variables is zero. In order to obtain more accurate state estimates, the initial estimates obtained from the state forecasting are utilized as measurements with finite Gaussian noise. Thereafter, a robust extended Kalman filter based probabilistic method is iteratively invoked, which uses the noisy measurements obtained from SCADA and AMI data in CHEN. For this purpose, the state and the measurement matrices of the robust EKF are formulated as,

$$\boldsymbol{\alpha}^{(k)} = \begin{bmatrix} \boldsymbol{x}_e^{(k-1)} & \boldsymbol{x}_h^{(k-1)} \end{bmatrix}^T + \boldsymbol{w}^{(k)}; \boldsymbol{w}^{(k)} \sim \mathcal{N}(0, \boldsymbol{Q_k}) \tag{18}$$

$$\boldsymbol{\beta}^{(k)} = \boldsymbol{H}(\boldsymbol{\alpha}^{(k)}) + \boldsymbol{v}^{(k)}; \boldsymbol{v}^{(k)} \sim \mathcal{N}(0, \boldsymbol{\mathcal{R}_k}) \tag{19}$$

where $\alpha^{(k)}$ and $\beta^{(k)}$, denote state matrix and the measurement matrix, respectively, for the k_{th} sample, with k = 1, 2, … K. $w(k)$ is the process noise with covariance Q_k at k_{th} instant, and $v^{(k)}$ is the measurement noise with covariance $\mathcal{R}_k$ at k_{th} instant. In (19), $H(.)$ is a vector function which combines the vector functions (15)–(17) values at k_{th} instant as,

$$\boldsymbol{H}(\boldsymbol{\alpha}^{(k)}) \equiv \begin{bmatrix} \boldsymbol{h}_{eS}^{(k)} & \boldsymbol{h}_{eA}^{(k)} & \boldsymbol{h}_{hS}^{(k)} & \boldsymbol{h}_{hA}^{(k)} & \boldsymbol{h}_{f}^{(k)} \end{bmatrix}^T \tag{20}$$

where, $\boldsymbol{h}_f^{(k)}$ denotes the forecasted values of the states taken as approximate measurements with relatively high error covariance. Since the system (18)–(19) is quasi-static system, the states of the system are updated as follows [41],

$$\boldsymbol{K}_k = \hat{\boldsymbol{P}}_{\boldsymbol{k}} \boldsymbol{\mathcal{J}}^{\boldsymbol{T}} \left[\boldsymbol{\mathcal{J}} \hat{\boldsymbol{P}}_{\boldsymbol{k}} \boldsymbol{\mathcal{J}}^{\boldsymbol{T}} + \boldsymbol{\mathcal{R}_k} \right] \tag{21}$$

$$\boldsymbol{\mathcal{J}} = \frac{\partial \boldsymbol{H}(\boldsymbol{\alpha}^{(k)})}{\partial \boldsymbol{\alpha}^{(k)}}_{\boldsymbol{\alpha}^{(k)} = \hat{\boldsymbol{\alpha}}^{(k)}} \tag{22}$$

$$\hat{\boldsymbol{\alpha}}^{(k+1)} = \hat{\boldsymbol{\alpha}}^{(k)} + \boldsymbol{K}_k (\boldsymbol{\beta}^{(k+1)} - \boldsymbol{H}(\hat{\boldsymbol{\alpha}}^{(k)})) \tag{23}$$

Thus the estimated state vector $\hat{\boldsymbol{\alpha}}^{(k+1)}$ results the final output of the system. $\boldsymbol{K_k}$ is the Kalman gain and $\boldsymbol{\mathcal{J}}$ is the Jacobian matrix of the filter, that relates the different measurements and the states in CHEN. The diagonal and off-diagonal elements of the Jacobian matrix are evaluated based on both inter-network and the coupling-network relations. The evaluation of the elements of Jacobian matrix is described as follows.

$$\boldsymbol{\mathcal{J}} = \begin{bmatrix} \boldsymbol{J}_e & \boldsymbol{J_{eh}} \\ \boldsymbol{J_{he}} & \boldsymbol{J}_h \\ & \boldsymbol{I_{s\times s}} \end{bmatrix} = \begin{bmatrix} \frac{\partial \boldsymbol{P}}{\partial \boldsymbol{\theta}} & \frac{\partial \boldsymbol{P}}{\partial |\boldsymbol{V}|} & \frac{\partial \boldsymbol{P}}{\partial \dot{\boldsymbol{m}}} & \frac{\partial \boldsymbol{P}}{\partial \boldsymbol{T}} \\ \frac{\partial \boldsymbol{Q}}{\partial \boldsymbol{\theta}} & \frac{\partial \boldsymbol{Q}}{\partial |\boldsymbol{V}|} & \frac{\partial \boldsymbol{Q}}{\partial \dot{\boldsymbol{m}}} & \frac{\partial \boldsymbol{Q}}{\partial \boldsymbol{T}} \\ \frac{\partial \boldsymbol{I}_f}{\partial \boldsymbol{\theta}} & \frac{\partial \boldsymbol{I}_f}{\partial |\boldsymbol{V}|} & \frac{\partial \boldsymbol{I}_f}{\partial \dot{\boldsymbol{m}}} & \frac{\partial \boldsymbol{I}_f}{\partial \boldsymbol{T}} \\ \frac{\partial \boldsymbol{\Phi}}{\partial \boldsymbol{\theta}} & \frac{\partial \boldsymbol{\Phi}}{\partial |\boldsymbol{V}|} & \frac{\partial \boldsymbol{Phi}}{\partial \dot{\boldsymbol{m}}} & \frac{\partial \boldsymbol{\Phi}}{\partial \boldsymbol{T}} \\ \frac{\partial \boldsymbol{T}}{\partial \boldsymbol{\theta}} & \frac{\partial \boldsymbol{T}}{\partial |\boldsymbol{V}|} & \frac{\partial \boldsymbol{T}}{\partial \dot{\boldsymbol{m}}} & \frac{\partial \boldsymbol{T}}{\partial \boldsymbol{T}} \\ & & \boldsymbol{I_{s\times s}} & \end{bmatrix} \tag{24}$$

In (24), the inter-electric submatrices include $\frac{\partial \boldsymbol{P}}{\partial \boldsymbol{\theta}}$, $\frac{\partial \boldsymbol{P}}{\partial |\boldsymbol{V}|}$, $\frac{\partial \boldsymbol{Q}}{\partial \boldsymbol{\theta}}$, $\frac{\partial \boldsymbol{Q}}{\partial |\boldsymbol{V}|}$, $\frac{\partial \boldsymbol{I}_f}{\partial \boldsymbol{\theta}}$ and $\frac{\partial \boldsymbol{I}_f}{\partial |\boldsymbol{V}|}$. The elements of these sub-matrices are computed using the relations (7)–(9). Similarly, the inter-heat sub-matrices include $\frac{\partial \boldsymbol{Phi}}{\partial \dot{\boldsymbol{m}}}$, $\frac{\partial \boldsymbol{\Phi}}{\partial \boldsymbol{T}}$, $\frac{\partial \boldsymbol{T}}{\partial \dot{\boldsymbol{m}}}$ and $\frac{\partial \boldsymbol{T}}{\partial \boldsymbol{T}}$. The elements of these sub-matrices are computed using the relations (2)–(6). Moreover, the matrix $\boldsymbol{I_{s\times s}}$ is an identity matrix of size equal to number of states, 's'. Out of the remaining sub-matrices which are off-diagonal, it can be identified that the submatrices $\frac{\partial \boldsymbol{P}}{\partial \boldsymbol{T}}$, $\frac{\partial \boldsymbol{Q}}{\partial \dot{\boldsymbol{m}}}$, $\frac{\partial \boldsymbol{Q}}{\partial \boldsymbol{T}}$, $\frac{\partial \boldsymbol{I}_f}{\partial \dot{\boldsymbol{m}}}$, $\frac{\partial \boldsymbol{I}_f}{\partial \boldsymbol{T}}$, $\frac{\partial \boldsymbol{T}}{\partial \boldsymbol{\theta}}$ and $\frac{\partial \boldsymbol{T}}{\partial |\boldsymbol{V}|}$ hold 'zero' values as there is no cross coupling between the corresponding states and the measurements. For $\boldsymbol{J_{eh}}$, the vector of the nonzero elements $\frac{\partial P_{1,source}}{\partial \dot{m}}$ is calculated using (4) and (10) as,

$$\frac{\partial P_{i,source}}{\partial \dot{m}} = \frac{\partial P_{i,CHP}}{\partial \dot{m}} = C_p A_{i,source} \frac{(T_{si,source} - T_{ri,source})}{c_{mi}} \tag{25}$$

Furthermore, in grid-connected mode, the off-diagonal submatrices $\frac{\partial \boldsymbol{\Phi}}{\partial \boldsymbol{\theta}}$ and $\frac{\partial \boldsymbol{\Phi}}{\partial |\boldsymbol{V}|}$ are zero, because the heat power is not a function of the electricity network and thus $\boldsymbol{J_{eh}} = \boldsymbol{0}$ [24]. In islanded mode, $\boldsymbol{J_{eh}}$ holds nonzero elements and the vector of the nonzero elements is calculated using (7) and (10) as,

$$\begin{bmatrix} \frac{\partial \boldsymbol{\Phi}_{i,source}}{\partial \theta_k} & \frac{\partial \boldsymbol{\Phi}_{i,source}}{\partial |V|_k} \end{bmatrix} = c_{mi} \left[Re(jV_i V_k^*)(G_{ik} - jB_{ik}) \quad Re(-V_i (G_{ik} - jB_{ik}) e^{-j\theta_k}) \right] \tag{26}$$

In (26), subscript 'i' represents the source at the electricity slack bus-bar. After the evaluation of Jacobian matrix, the state matrix ($\boldsymbol{\alpha}^{(k+1)}$) of CHEN is updated using (21)–(23). Finally, the error covariance vector $\hat{P}_{k+1}$ is for the next iteration is updated as follows.

$$\hat{\boldsymbol{P}}_{\boldsymbol{k+1}}^{-} = \hat{\boldsymbol{P}}_{\boldsymbol{k}} + \boldsymbol{Q_k} \tag{27}$$

$$\hat{\boldsymbol{P}}_{\boldsymbol{k+1}} = \hat{\boldsymbol{P}}_{\boldsymbol{k+1}}^{-} - \boldsymbol{K_k} \boldsymbol{\mathcal{J}} \hat{\boldsymbol{P}}_{\boldsymbol{k+1}}^{-} \tag{28}$$

The matrices $\boldsymbol{\mathcal{R}_k}$ and $\boldsymbol{Q_k}$ in the process are typically initialized as $10^{-4}\boldsymbol{I_s}$ and $10^{-4}\boldsymbol{I_m}$, respectively [42], where subscripts 's' and 'm' denote number of states and number of measurements respectively. In (21), however, $\boldsymbol{\mathcal{R}_k}$ is replaced with $\boldsymbol{\mathcal{R}_k} e^{\|(\boldsymbol{\beta}^{(k+1)} - \boldsymbol{H}(\boldsymbol{\alpha}^{(k)})\|^2}$, by assigning the exponential term of error between the sensed and the calculated measurements. If the error is high, then, the exponential factor increases faster, which increases the error covariance term and thereby mitigation of the error is achieved. Thus, robust performance is achieved by incorporating exponential term, under high measurement noises.

4. Results and discussion

The proposed method is tested on a Barry Island test system as shown in Fig. 4. It consists of a heat network with a total of 31 pipes and 29 load nodes, and an electrical distribution network with a total of 8 buses with lumped loads at 6 buses. Both the networks are coupled through the CHP units. The detailed parameters of the test system considered are reported in [24]. The load data for all the heat network nodes and electric load buses in the CHEN are altered to obtain different operating conditions, and the load flow analysis of the combined network is carried in the Matlab® platform, to obtain various measurements with the operating conditions. For instance, the set of SCADA and AMI measurements obtained under different operating conditions at different instants in a 2-day interval are as shown Figs. 5(a) and 5(b) respectively at 15 min. and hourly intervals. A total of 10000 operating conditions under different load conditions are considered, i.e., 10000 samples are simulated to acquire the training and testing data sets. Out of these, 20% (i.e.2000) samples are considered for testing purpose. The simulated measurements (which include both SCADA and AMI measurements) in various operating conditions are superimposed with white Gaussian noise [17], to test the effectiveness of the state-estimation with proposed algorithm. The different test cases considered are as follows.

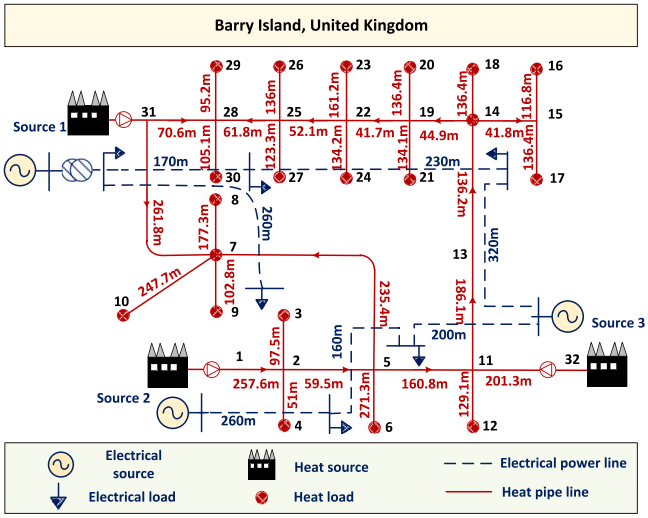

Fig. 4. Barry Island test system.

- Case-I: Effectiveness of the DNN based state forecasting with SCADA measurements
- Case-II: Effectiveness of the proposed hybrid method with both SCADA and AMI measurements
- Case-III: Comparison of the hybrid method with the conventional state estimation method
- Case-IV: Evaluation of the hybrid method under the presence of bad-data in the measurements
- Case-V: Evaluation of the Computational burden of the algorithm

4.1. Case-I: Effectiveness of DNN based state forecasting

Initially, effectiveness of the state-forecasting method employed in this work, is presented. The training data-sets used for state-forecasting are reported in Section 2, where the input data is the partial SCADA measurements, and the output data is the forecasted states of the system. These forecasted states of the system include voltage magnitude, voltage phase angle, pipe mass flow rate, supply temperature and return temperatures at load nodes. The forecasting is being carried out using the DNN algorithm with the procedure as shown in Fig. 3. The results of various forecasted states, are compared with the ideal states, to give the forecast error. The AMFE over different operating conditions, is as reported in Fig. 6, where the AMFEs in the supply and return temperatures at all the load nodes, mass flow rates in all the pipes, voltage magnitudes at all load buses and voltage angles at all buses except the slack bus are shown. Moreover, the DNN phase is substituted with the single-layer ANN in Fig. 1, and the corresponding variation in the mean error is also pointed out in Fig. 6. Furthermore, Fig. 7 points out the maximum and the mean of AMFEs of various forecasted states using DNN (e.g., mean and the maximum of the return temperature AMFEs over all the load nodes, is as shown in the last couple of bars in Fig. 7). It can be seen that the AMFEs obtained from the initial forecasting stage are sufficiently low, e.g. below about 0.5% error in each of the forecasted state. Thus presented DNN algorithm suffices for nearly accurate estimates of different states in CHEN, solely based on SCADA measurements in the absence of AMI measurements.

4.2. Case-II: Effectiveness of hybrid state-estimation method

In this case, the measurements data is considered from both SCADA and AMI measurements. After the initial forecasting stage with the DNN based method, using the SCADA measurements, the robust EKF-based hybrid estimator is applied as shown in Fig. 1, which makes use of AMI measurements. As the AMI measurements are not always available, the hybrid estimator is employed only at the instants where both SCADA and AMI measurements are readily available, as identified in Fig. 2. The hybrid estimator has the information of all the measurements and the forecasted states for quick convergence, and using them, the accurate system state estimates are obtained through the procedure highlighted in Section 3. Since the robust EKF involves modeling equations, to ensure the system observability, some pseudo measurements need to be considered along with the available partial SCADA and AMI measurements. The pseudo measurements in this case are simulated by appending 50% Gaussian noise to the simulated measurements at various operating conditions. Thus, the pseudo measurements of nodal heat power consumptions, load outlet temperatures, active and reactive powers at various load nodes and buses are considered herein, with varying degrees of system observability. For instance, with high system observability with available SCADA and AMI measurements, 10% of pseudo measurements are considered. With low system observability, 50% of pseudo measurements are considered, i.e. half of the total number of measurements of the measurement set highlighted in the Section 3.2 are considered. For fair comparison with the DNN based state-forecasting method, the set of SCADA measurements are maintained the same, while the AMI measurements are increased to increase the system observability. Fig. 8 illustrates the mean and maximum values of AMEEs of the CHEN states, under 10%, 25% and 50% pseudo measurements, while the mean and maximum values of AMFEs with DNN are also presented. It can be observed that the values of AMEEs are higher for 50% pseudo-measurements as compared with the 25% and 10% pseudo-measurements. As the percentage of pseudo-measurements are increased, the AMEEs are noticeably increased due to having higher degree of uncertainty in the state estimation. On the other hand the AMFEs with the DNN, which is solely based on SCADA measurements, tend to be lower than considering the EKF based hybrid state estimator with greater than 25% of pseudo measurements.

4.3. Case-III: Comparison of hybrid method with conventional state-estimation

Conventionally, the CHEN state estimators proposed do not include the state forecasting stage, and the state estimation is performed either with traditional least squares based methods (e.g., WLS and WLAV based) [18]. In contrast to the proposed hybrid CHEN state estimator, the conventional state estimators are purely model based approaches, which require mathematical modeling the electric and heat network dynamics and demand the system to be observable. Consequently the model based methods cannot be relied upon in the CHEN, where the measurement redundancy is low. Thus the traditional WLS/WLAV-based approaches are not robust methods for CHEN state estimation. Therefore, for fair comparison between the traditional model-based estimator and the proposed hybrid estimator, a high degree of system observability is kept with only 10% pseudo measurements in AMI data. The estimated CHEN states with the proposed hybrid estimator and the model-based WLS estimator, are observed at different test instants. The error histogram of the mean of the estimated AMEEs is plotted and presented in Fig. 9. For ease of understanding, the absolute error chart is plotted for the mean of the different states in the electrical network and the heat network. Y-axis represents the number of instances/data frequency, while the X-axis represents the mean of the estimated error. For instance, the mean of the voltage estimation error over all the electrical voltage buses, with proposed hybrid method is near zero for over 1400 data instances as depicted in Fig. 9(a). Fig. 9(a) represents the error histogram with the electrical network states (e.g., voltage magnitude and voltage phase angle), while Fig. 9(b) represents the error histogram with the heat network states. The summary statistics depicting the approximate mean and standard deviations with the absolute error values depicted in the histogram plots are also reported

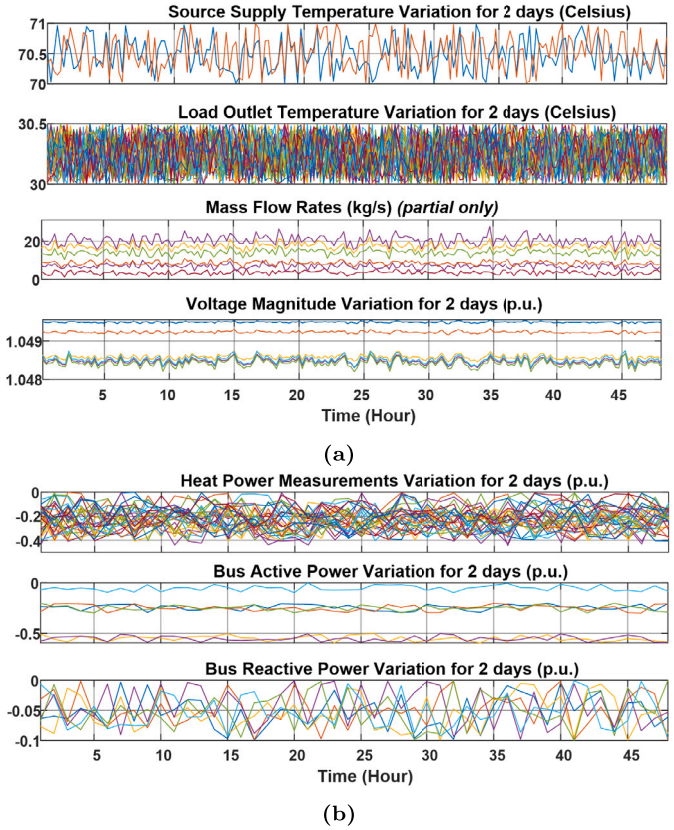

Fig. 5. Measurements simulated with different operating conditions in 2-day interval: (a) SCADA Measurements and, (b) AMI Measurements.

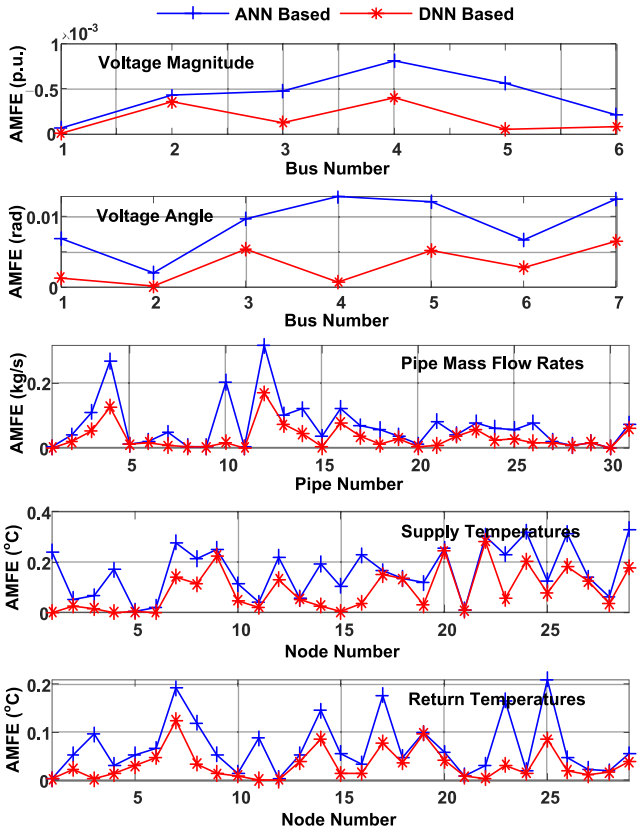

Fig. 6. AMFEs of the Forecasted CHEN States using DNN and ANN.

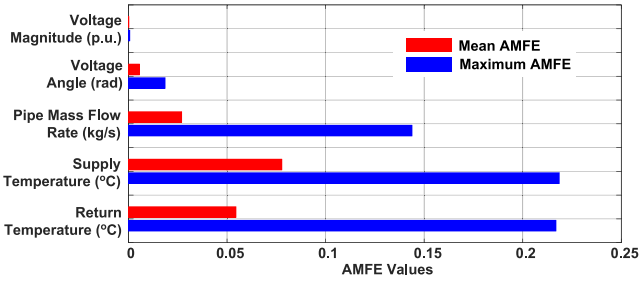

Fig. 7. Mean and the Maximum of AMFEs of the Forecasted CHEN States using DNN.

herein. The mean values of different quantities are reported in Table 1 and the standard deviation values of as reported in Table 2. Thus, it is observed that the hybrid state estimator ascertains more accuracy than the traditional model based estimator, in case of the less observable systems such as CHEN.

4.4. Case-IV: Effectiveness of hybrid method under presence of bad-data

As mentioned earlier, the AMI measurements data is considered from the set of simulated measurements with 2% Gaussian error distribution. To evaluate the robustness of the hybrid method under the presence of some bad data in the measurements, the AMI measurements of active and reactive power measurement data at electrical bus-4 and heat power measurement data at bus-5 are added with the erroneous data with five times the normal noise, during the time instants between 60 to 80 h. Consequently, Fig. 10(a) and Fig. 10(b) depict a close look upon the comparison of proposed hybrid estimator with the traditional WLS method. As seen in Fig. 10, WLS based estimator provides more biased state estimates of bus voltages and angles at bus-4, while the

Table 1
Mean values of absolute errors of model-based estimator and proposed estimator.

Method	Voltage magnitude (p.u.)	Voltage angle (rad)	Mass flow rate (kg/s)	Supply temperature (°C)	Return temperature (°C)
Model-based WLS	0.0002	−0.00004	−0.0012	0.0901	0.0108
Proposed	0.0003	−0.00005	−0.0013	0.0409	0.0045

Table 2
Standard deviation values of the absolute errors of the model-based estimator and the proposed estimator.

Method	Voltage magnitude (p.u.)	Voltage angle (rad)	Mass flow rate (kg/s)	Supply temperature (°C)	Return temperature (°C)
Model-based WLS	0.0067	0.0004	0.0341	0.1042	0.0536
Proposed	00.0031	0.0001	0.0148	0.0600	0.0293

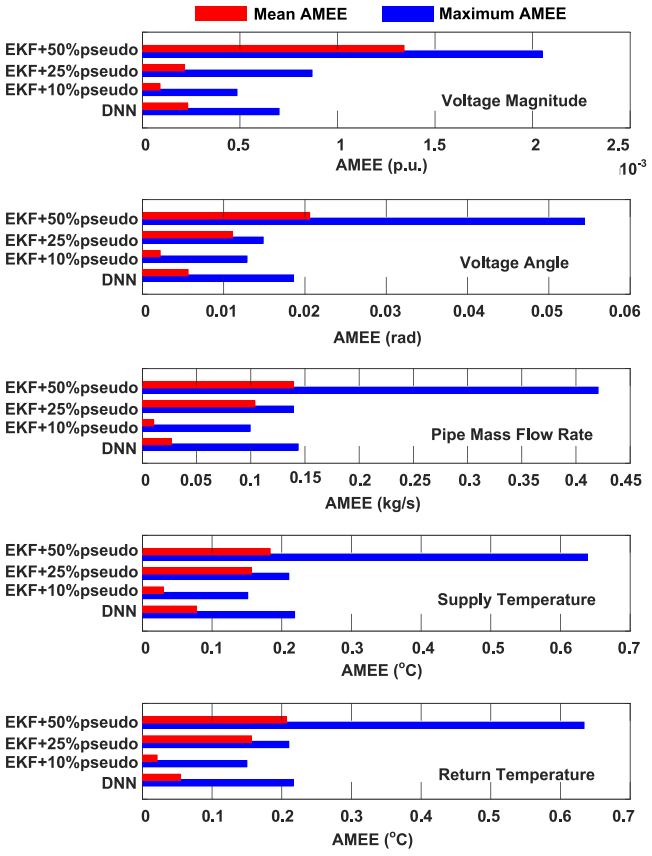

Fig. 8. Mean and Maximum of AMEEs of Estimated CHEN States using EKF with varying pseudo measurements.

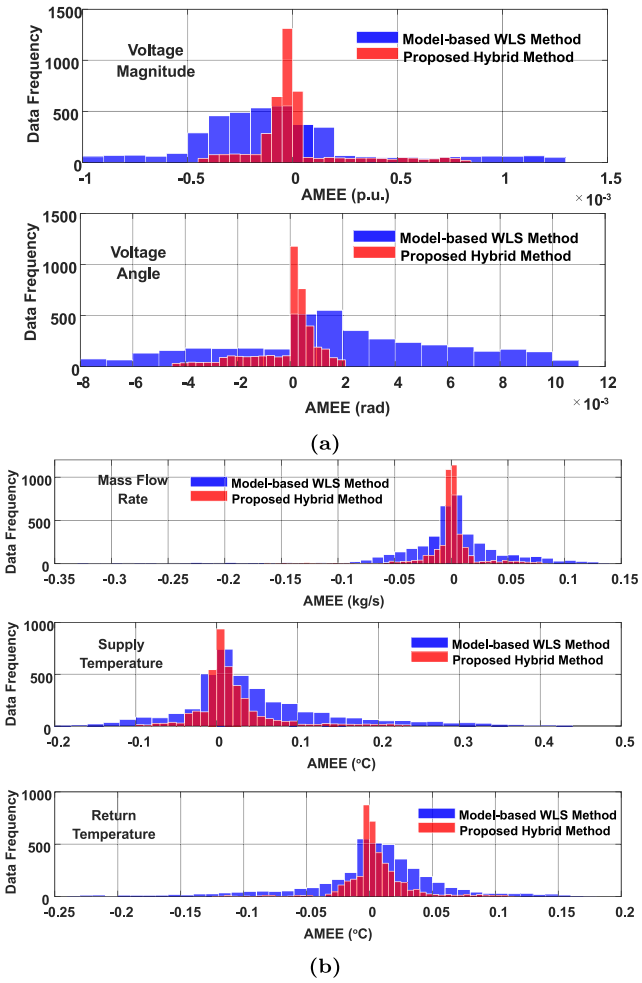

Fig. 9. Comparison of absolute errors between model-based estimator and proposed hybrid estimator (a) Electric network states (b) Heat network states.

mass flow rate, supply and return temperatures in the heat network are also biased. Further, the robustness of the hybrid method under the presence of some gross errors in the SCADA measurements is simulated, where the voltage magnitudes at the electric buses are added with the erroneous data with five times the normal noise, during the time instants between 35 to 50 h. Consequently, Fig. 11 depicts the comparison of the proposed hybrid estimator with the traditional WLS method. The WLS based estimator provides more biased state estimates of bus voltages and angles, compared to the hybrid state estimator. The hybrid estimator is robust against the bad-data, because the measurement redundancy and the convergence is increased on account of initial DNN based forecasted states.

4.5. Case-v: Evaluation of computational burden

For the evaluation of computational burden, the DNN-based estimator is triggered in fifteen minutes interval, while the EKF-based estimator is executed hourly, for about 72 h, with computer specifications holding i7 Intel processor and 32 GB RAM operated on Windows OS. Fig. 12 shows the time taken by various steps involved with the hybrid estimator. It may be noted that the DNN based state

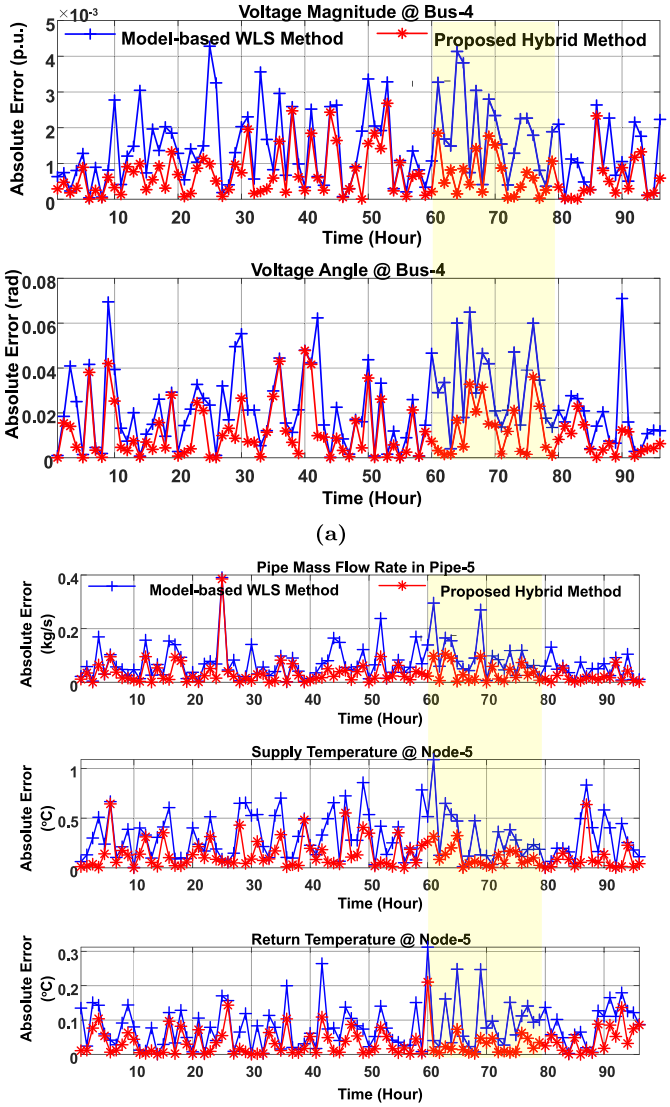

Fig. 10. Comparative analysis with bad AMI data (a) absolute errors in electric network states (bus-4 voltage magnitude and angle); (b) absolute errors in heat network states (mass flow rate in pipe-5, supply and return temperatures at node-5).

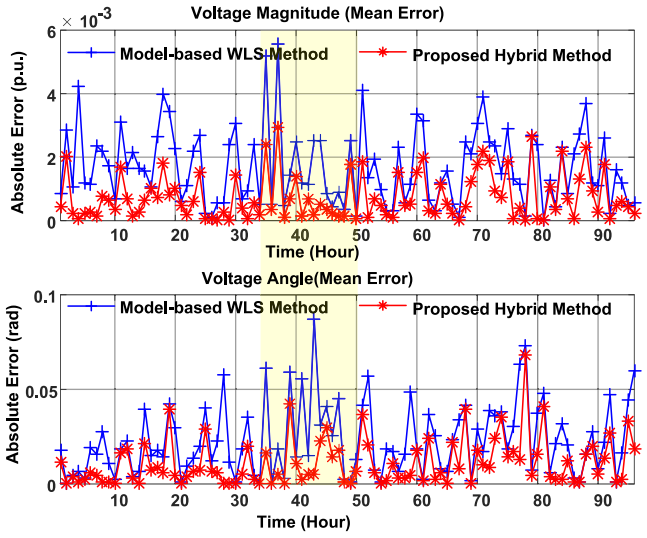

Fig. 11. Comparative analysis gross errors in SCADA measurements between certain time instants.

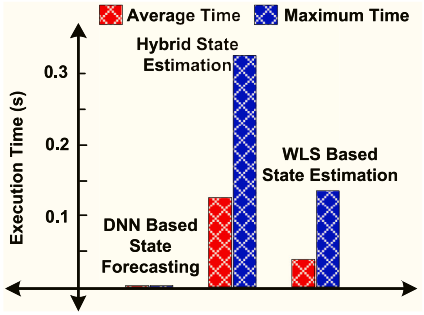

Fig. 12. Illustration of computational times for Barry Island system.

forecasting step (Section 2) involves least time as in the case with the data learning methods, while the EKF-based hybrid state estimation step (Section 3) takes significant computational time as it involves several matrix computations including the Jacobian matrix. While the model based WLS state estimator involves less computational time, yet, the proposed hybrid method is practically deployable as the state

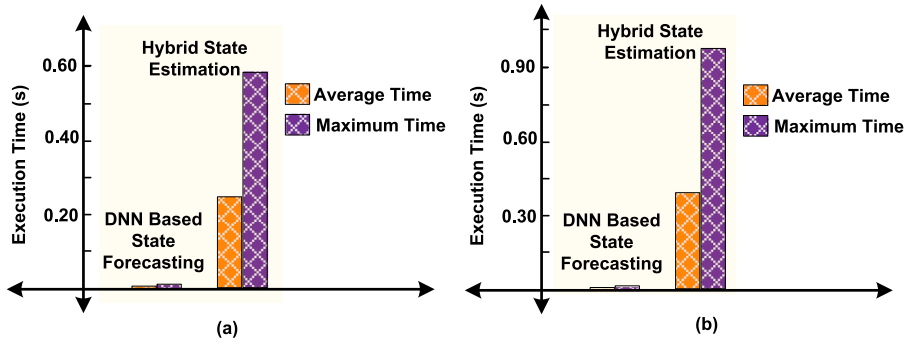

Fig. 13. Illustration of computational times for city-level CHEN system with (a) High computational specification (b) Low computational specification .

estimation in CHEN is usually performed in the order of minutes and the algorithm takes less than a second.

Further analysis on computational performance of the hybrid estimator is evaluated on 'city-level CHEN system' [43], consisting of a 19-bus electric power system and a 69-node heating system. For testing the scalability, evaluation of computational burden of this system is carried out with computer specifications holding 32 GB RAM and i7 Intel processor. The measurement data-set for the network is generated exactly in a similar way as that of Barry Island reported before Section 4.1. Here, the DNN-based estimator is triggered in fifteen minutes interval and the EKF-based estimator is executed hourly. Fig. 13(a) shows the computational results with the city-level CHEN system at both the steps involved with the proposed estimator. It may be noted that the DNN based state forecasting step involves least time as in the case with the data learning methods, while the EKF-based hybrid state estimation step takes significant computational time. Further, it is observed that the computational time has considerably increased (esp. with the Hybrid state estimation), as the system size has increased to the 19-bus and 69-node system. This is because the hybrid state estimator involves several matrix computations including a large size Jacobian matrix. When the same system simulation is carried out with computer specifications holding i5 Intel processor and only 16 GB RAM, the corresponding results are highlighted in Fig. 13(b). From the results, it is observed that the estimator functions considerably well even at a low computational cost; however, the computational time is increased. Therefore, the proposed estimator can easily extend up to the CHEN system sizes with 19-bus electric power system and a 69-node heating system.

5. Conclusions

A hybrid state estimation framework is presented herein, which precisely estimates the CHEN network states using the limited number of SCADA and AMI measurements data. Two step method is employed here, wherein the first step, i.e. the state-forecasting is performed at frequent intervals to give the approximate information of the network states to the operator. The second step is performed using robust extended Kalman filter at less frequent intervals, upon the availability of AMI data, to output the accurate system states even under the presence of bad-data in measurements. The method is tested on a Barry Island case study of the United Kingdom. About 10,000 operating scenarios are considered to set a comprehensive data-set, out of which 80% datasets are used for the DNN training purpose. The results show that AMFEs of the forecasted states are achieved below 0.5%, solely with the SCADA measurements. When both the SCADA and AMI information is processed through the hybrid estimator, the output AMEEs are observed to go down significantly, proving the effectiveness of the proposed framework. The test cases are considered with varying levels of redundancy in AMI measurements and accordingly 10%, 25% and 50% of pseudo measurements are added to ensure the system observability. It is observed that the hybrid estimator with more than 25% of pseudo measurements, is undesirable in the case study, as the state-forecasting performance supersedes the state estimator performance. Furthermore, the comparative analysis with the state-of-art model-based approaches, show the superior performance of the proposed hybrid estimator, as it involves the two step procedure with robust EKF based measurements processing strategy wherein the forecasted states are also treated as measurements with Gaussian/white noise. Due to this reason, it is also noticed that the bad-data injected in the electric and heat network measurements do not much effect the estimation accuracy with the proposed estimator. Finally the computational time of the proposed method is evaluated, wherein it has been noted that the DNN takes negligible amount of time whereas the EKF based method takes as significant computational time. However, the computational time of approach is observed to be quite low compared to the field state estimators, which run every few minutes. Moreover, the proposed framework does not rely on the system model at different instants, unlike different state-of-art CHEN state estimation methods. Consequently, the proposed framework serves as a suitable solution for the state-estimation needs of the current day CHEN network bearing highly redundant measurements.

Declaration of competing interest

The authors declare that they have no known competing financial interests or personal relationships that could have appeared to influence the work reported in this paper.

Data availability

Data will be made available on request.

Acknowledgments

This work was supported in part by EnergyREV under Grant EP/S031863/1, in part by MC2 under Grant EP/T021969/1, and in part by "Supergen Energy Networks Hub" under Grant EP/S00078X/1, through the Engineering and Physical Sciences Research Council (EPSRC). The authors would also like to acknowledge SERB National Science Chair Fellowship, Start-up Research Grant with SRG/2023/000410, Government of India, and Faculty Research Scheme Grant FRS(168)/2021-2022/EE.

References

[1] Backe S, Korpås M, Tomasgard A. Heat and electric vehicle flexibility in the European power system: A case study of norwegian energy communities. Int J Electr Power Energy Syst 2021;125:106479.
[2] Tian H, Zhao H, Liu C, Chen J, Wu Q, Terzija V. A dual-driven linear modeling approach for multiple energy flow calculation in electricity–heat system. Appl Energy 2022;314:118872.
[3] Jayasuriya L, Chaudry M, Qadrdan M, Wu J, Jenkins N. Energy hub modelling for multi-scale and multi-energy supply systems. In: 2019 IEEE milan powertech. IEEE; 2019, p. 1–6.

[4] Huang M, Wei Z, Ju P, Wang J, Chen S. Incentive-compatible market clearing for a two-stage integrated electricity-gas-heat market. IEEE Access 2019;7:120984–96.
[5] Jiang T, Deconinck G, Wu J, Bai L, Bo R, Mu Y, et al. Guest editorial: Special issue on integrated local energy systems. Int J Electr Power Energy Syst 2023;148:108929.
[6] Zhang M, Wu Q, Rasmussen TBH, Yang X, Wen J. Heat pumps in Denmark: Current situation of providing frequency control ancillary services. CSEE J Power Energy Syst 2021.
[7] Chen Y, Lu X, Zhang H, Zhao C, Xu Y. Optimal configuration of integrated energy station using adaptive operation mode of combined heat and power units. Int J Electr Power Energy Syst 2023;152:109171.
[8] Huang B, Wang L, Wang R, Han R, Sun Q. A unified model for transient flow analysis of the integrated electric power and natural gas system with multiple time scales. Int J Electr Power Energy Syst 2022;142:108133.
[9] Vedantham LS, Zhou Y, Wu J. ICT infrastructure supporting smart local energy systems: A review. IET Energy Syst Integr 2022.
[10] Fathtabar H, Barforoushi T, Shahabi M. Dynamic long-term expansion planning of generation resources and electric transmission network in multi-carrier energy systems. Int J Electr Power Energy Syst 2018;102:97–109.
[11] Lan T, Strunz K. Droop control for district heating networks: Solution for temperature control of multi-energy system with renewable power supply. Int J Electr Power Energy Syst 2023;146:108663.
[12] Sheng T, Yin G, Wang B, Guo Q, Dong J, Sun H, et al. State estimation approach for combined heat and electric networks. CSEE J Power Energy Syst 2020.
[13] Aminifar F, Shahidehpour M, Fotuhi-Firuzabad M, Kamalinia S. Power system dynamic state estimation with synchronized phasor measurements. IEEE Trans Instrum Meas 2014;63(2):352–63.
[14] Kabiri M, Amjady N. A new hybrid state estimation considering different accuracy levels of PMU and SCADA measurements. IEEE Trans Instrum Meas 2019;68(9):3078–89.
[15] Sun K, Liu R, Huang M, Wei Z, Duan F, Sun G. Real-time recursive correction state estimation utilizing only SCADA measurements. In: 2021 IEEE 5th conference on energy internet and energy system integration. IEEE; 2021, p. 2473–7.
[16] Li J, Zhu M, Huang Y. Classification and location scheme selection of coupling components in integrated electrical and heating systems with renewable energy. CSEE J Power Energy Syst 2019;6(3):619–29.
[17] Zhang S, Gu W, Qiu H, Yao S, Pan G, Chen X. State estimation models of district heating networks for integrated year=2021, energy system considering incomplete measurements. Appl Energy 282:116105.
[18] Zang H, Geng M, Xue M, Mao X, Huang M, Chen S, et al. A robust state estimator for integrated electrical and heating networks. IEEE Access 2019;7:109990–10001.
[19] Huang M, Wei Z, Sun G, Zang H. Hybrid state estimation for distribution systems with AMI and SCADA measurements. IEEE Access 2019;7:120350–9.
[20] Chen Y, Yao Y, Zhang Y. A robust state estimation method based on SOCP for integrated electricity-heat system. IEEE Trans Smart Grid 2020;12(1):810–20.
[21] Du Y, Zhang W, Zhang T. ADMM-based distributed state estimation for integrated energy system. CSEE J Power Energy Syst 2019;5(2):275–83.
[22] Zhang T, Li Z, Wu Q, Zhou X. Decentralized state estimation of combined heat and power systems using the asynchronous alternating direction method of multipliers. Appl Energy 2019;248:600–13.
[23] Wang C, Gong Z, Liang Y, Wei W, Bi T. Data-driven wind generation admissibility assessment of integrated electric-heat systems: A dynamic convex hull-based approach. IEEE Trans Smart Grid 2020;11(5):4531–43.
[24] Liu X, Wu J, Jenkins N, Bagdanavicius A. Combined analysis of electricity and heat networks. Appl Energy 2016;162:1238–50.
[25] Yang J, Zhang N, Botterud A, Kang C. On an equivalent representation of the dynamics in district heating networks for combined electricity-heat operation. IEEE Trans Power Syst 2019;35(1):560–70.
[26] Huang S-C, Lu C-N, Lo Y-L. Evaluation of AMI and SCADA data synergy for distribution feeder modeling. IEEE Trans smart Grid 2015;6(4):1639–47.
[27] He X, Li C, Du M, Dong H, Li P. Hybrid measurements-based fast state estimation for power distribution system. IEEE Access 2021;9:21112–22.
[28] Wang S, Liu G, Huang R, Qin S. State estimation method for active distribution networks under environment of hybrid measurements with multiple sampling periods. Autom Electr Power Syst 2016;40(19):30–6.
[29] Göl M, Abur A. A hybrid state estimator for systems with limited number of PMUs. IEEE Trans Power Syst 2014;30(3):1511–7.
[30] Kong X, Chen Y, Xu T, Wang C, Yong C, Li P, et al. A hybrid state estimator based on SCADA and PMU measurements for medium voltage distribution system. Appl Sci 2018;8(9):1527.
[31] Costa AS, Albuquerque A, Bez D. An estimation fusion method for including phasor measurements into power system real-time modeling. IEEE Trans Power Syst 2013;28(2):1910–20.
[32] Sheng T, Yin G, Guo Q, Sun H, Pan Z. A hybrid state estimation approach for integrated heat and electricity networks considering time-scale characteristics. J Mod Power Syst Clean Energy 2020;8(4):636–45.
[33] Feng X, Yang F, Peterson W. A practical multi-phase distribution state estimation solution incorporating smart meter and sensor data. In: 2012 IEEE power and energy society general meeting. IEEE; 2012, p. 1–6.
[34] de Souza GP, do Couto Boaventura W. Time-alignment of electrical network measurements through time series of cycle RMS values. Int J Electr Power Energy Syst 2023;144:108518.
[35] Blakely L, Reno MJ, Ashok K. AMI data quality and collection method considerations for improving the accuracy of distribution models. In: 2019 IEEE 46th photovoltaic specialists conference. IEEE; 2019, p. 2045–52.
[36] Zhang L, Wang G, Giannakis GB. Real-time power system state estimation and forecasting via deep unrolled neural networks. IEEE Trans Signal Process 2019;67(15):4069–77.
[37] Muscas C, Pau M, Pegoraro PA, Sulis S. Effects of measurements and pseudomeasurements correlation in distribution system state estimation. IEEE Trans Instrum Meas 2014;63(12):2813–23.
[38] Steer K, Wirth A, Halgamuge S. Control period selection for improved operating performance in district heating networks. Energy Build 2011;43(2–3):605–13.
[39] Cataliotti A, Cervellera C, Cosentino V, Di Cara D, Gaggero M, Macciò D, et al. An improved load flow method for MV networks based on LV load measurements and estimations. IEEE Trans Instrum Meas 2018;68(2):430–8.
[40] Zhao J, Netto M, Huang Z, Yu SS, Gómez-Expósito A, Wang S, et al. Roles of dynamic state estimation in power system modeling, monitoring and operation. IEEE Trans Power Syst 2021;36(3):2462–72.
[41] Lakshmi S, Singh B, Mishra S. Fault ride-through strategy for two-stage grid-connected photovoltaic system enabling load compensation capabilities. IEEE Trans Ind Electron 2019;66(11):8913–24.
[42] Anagnostou G, Pal BC. Derivative-free Kalman filtering based approaches to dynamic state estimation for power systems with unknown inputs. IEEE Trans Power Syst 2017;33(1):116–30.
[43] Qin X, Shen X, Guo Y, Pan Z, Guo Q, Sun H. Combined electric and heat system testbeds for power flow analysis and economic dispatch. CSEE J Power Energy Syst 2020;7(1):34–44.